Star Formation in Superthin Galaxies

Ganesh Narayanan[1]* and Arunima Banerjee[2]†
{1, 2} *Indian Institute of Science Education and Research, Tirupati 517507, India*

12 April 2021

ABSTRACT

Superthin galaxies (STs) are low surface brightness galaxies (LSBs) (central surface brightness in B-band > 23 magarcsec^{-2}) with a strikingly high planar-to-vertical axes ratio of $\sim 10-20$ with no bulge component. The superthin vertical structure of STGs results in significantly lower values of disc dynamical stability (Jog 1992) and hence higher values of the predicted SFR compared to face-on LSBs. We systematically study the star formation rate (SFR) of samples of STGs and LSBs and compare their relative values. Using GALEX FUV, we estimate the SFR of 212 STGs and 158 LSBs, the median values being 0.057 $M_\odot/yr$ and 0.223 $M_\odot/yr$ respectively. We next obtain the SFR from WISE (W3) of 549 STGs and 345 LSBs, with median values of 0.471 $M_\odot/yr$ and 0.17 $M_\odot/yr$ respectively. Finally, from SED fitting of photometric data in ten bands (FUV, NUV of GALEX, u,g,r,i,z of SDSS & J, H, Ks of 2MASS) in MAGPHYS, we find the SFR for a sample of 65 STGs and 103 LSBs to be 0.357 $M_\odot/yr$ and 0.616 $M_\odot/yr$ respectively. Also, as is indicated by the median values of number of bursts after $t_{\rm form} = 1$ and an exponential star formation time scale parameter $\gamma = 0.2$ Gyr^{-1}, the SFR remains fairly constant over time. Interestingly, in spite of having low SFR compared to ordinary star-forming galaxies, both superthins and LSBs populate the star forming blue cloud region in the specific star formation (sSFR) - stellar mass (M*) plane of galaxies.

Key words: galaxies: star formation, galaxy: evolution, ultraviolet: stars, galaxies: spiral, galaxies: disc

1 INTRODUCTION

Superthin galaxies (STs) are bulgeless low surface brightness disc galaxies with strikingly high planar-to-vertical axes ratio ($a/b \sim 10 - 20$) (Matthews et al. 1999a). Low Surface Brightness galaxies (LSBs), in turn, are galaxies with central B-band surface brightness $\mu_B > 23$ mag arcsec^{-2} (Bothun et al. 1997; Schombert et al. 2001), or alternatively, with central R-band surface brightness $\mu_B > 24$ mag arcsec^{-2} (Courteau 1996; Adami et al. 2006). They are gas-rich and dark matter dominated with low star formation rates (SFRs), and therefore constitute proxies for a primeval galaxy population in the local universe (van der Hulst et al. 1993; Bothun et al. 1997; McGaugh 1994; de Blok et al. 1995; van der Hulst et al. 1993; van den Hoek et al. 2000; Bell et al. 2000).

The average SFRs of LSBs is lower by at least an order of magnitude than HSBs (Bothun et al. 1997). Further these galaxies are bluer in color ($U - B < 0$) when compared to high surface brightness galaxies (HSBs) (de Blok et al. 1995; McGaugh & Bothun 1994), possibly indicating a predominantly young stellar population (Bell et al. 1999; de Blok et al. 1995). However, the age-metallicity degeneracy poses a challenge in determining age from galaxy colors (Worthey 1994). In any case, from bluer optical colors of LSBs, de Blok et al. (1995) ruled out various scenarios

such as a disc-fading, an initial starburst, an exponentially declining or a constant star formation rate (SFR) in the star formation history (SFH) of LSBs. van den Hoek et al. (2000) in turn showed that LSBs have an exponentially decreasing SFRs, and follow same evolutionary history as HSBs, but at a slower rate with only a few star formation bursts is required to explain blue color of LSBs. However, there exists a large fraction of population of red LSBs which do not fit into the proposed model for the formation of blue LSBs (O'Neil et al. 2008). Besides, current SFRs of LSBs are generally higher than their past SFRs, which is again indicative of a young stellar population, and which may possibly be attributed to a late epoch of formation or a slow paced evolution. A recent study with H_α luminosity for 357 LSBs showed that the sample has a lower global SFR($log(SFR)(M_\odot yr^{-1}) = -1.5$) and lower star formation density($log(\Sigma_{SFR})(M_\odot yr^{-1} kpc^{-2}) = -3.3$) relative to HSBs (Lei et al. 2019). Lee et al. (2009) found an median SFR of 0.003 $M_\odot yr^{-1}$ for a sample of 300 dwarf galaxies; H_α traces the star formation rate in the last 3-10 Myrs. Interestingly, in simulations Zackrisson et al. (2005) found their sample LSBs do not appear to have formed stars over cosmological time scales even with constant or increasing SFRs and also argued that LSBs formation epochs are too ambiguous to decide even with these correlations. And if LSBs are formed $2 \sim 4$ Gyrs ago, then it challenges the model of galaxy formation in the λCDM cosmology (Zackrisson et al. 2005).

---

* E-mail: ganeshn@students.iisertirupati.ac.in
† E-mail : arunima@iisertirupati.ac.in

In this paper, we compare and contrast the SFRs of STs and LSBs in general. From a dynamical perspective, the superthin vertical structure of the stellar disc in STs should result in a lower disc dynamical stability and hence a higher star formation rate compared to that of general LSBs (See, for example, Jog (1996)). We estimate the SFR using FUV luminosity from GALEX & NIR from WISE for a sample of STs and LSBs. FUV traces the emission from young stellar populations (100 Myrs) and estimates the recent star formation rate in the galaxy which however is highly sensitive to dust extinction. WISE NIR similarly gives SFR by tracing a young stellar population (100 Myr) but is relatively unaffected by dust extinction effects. To better constrain other physical parameters related to star formation, we need photometric data in other bands (GALEX (NUV, FUV), SDSS (u,g,r,i,z) and NIR (J,H,Ks)) as well to construct the SED whch is subsequently fitted by the model SEDs predicted by the evolutionary synthesis models.

The rest of the paper is organized as follows. In §2, we describe how the SFR is determined using different tracers namely the FUV emission, the NIR emission. We further determine the SFR of our sample STs and LSBs using Spectral Energy Disribution (SED) fitting. In §3, we describe our sample and in §4, the observational constraints for the SED fitting. In §5, we present our results followed by discussion and conclusions in §6 and 7 respectively.

2 SFR TRACERS

2.1 SFR : FUV (GALEX) and NIR (WISE)

Because of the deep sensitivity, wide field-of-view, GALEX observations are suitable for studying star formation properties of outer galaxy disks, tidal tails, LSBs and dwarf Irregular galaxies (Bianchi 2011). Young massive stars are tracers for recent star formation activities in the galaxy and are also bright in UV in distant galaxies. UV traces a stellar population of 100 Myrs order compared to $H\alpha$(Murphy et al. 2011; Hao et al. 2011). UV is also highly sensitive to dust extinction which plays an important role in star formation.

SFR/L_u varies over a magnitude for range of galaxy colors, L_u being the luminosity in the u-band. Although integrated colors gives a better estimate of the SFR, they may not be robust to the choice of the initial mass function (IMF), dust content, age, metallicity and star formation history. In UV, SFR scales linearly with luminosity dominated by spectrum of young stars as given by

$$SFR(M_\odot yr^-1) = 1.4 * 10^{-26} L_\nu (erg s^{-1} Hz^{-1}) \tag{1}$$

(Kennicutt 1998). In deriving the above relation, it was assumed that the SFR remained constant for time scale larger compared to age of dominant UV emitting stars in continuous star formation approximation. The IMF chosen was the Salpeter IMF. This relation can only be used when the SFR is constant over timescales $> 10^8 yr$ and is also sensitive to the choice of IMF and extinction.

Magnitudes in WISE W3 ($12\mu m$) data were used to estimate SFR for both the sample of galaxies. WISE can give us dust free SFR estimate compared to UV SFR estimates.

Takeuchi et al. (2005) showed that the $12\mu m$ luminosity could be used as a reliable measure of total infrared luminosity and can be used for calibrating SFR. Any corrections for extinction in UV gives a large scatter in the SFR relation(Calzetti et al. 2007). WISE(W4) band is not contaminated by emission lines (z=0) and so in the absence of active galactic nucleus (AGN)activity, gives us a reliable measure of star formation comparable to $H\alpha$ measures (Brown et al. 2017). However, the widespread use of this band is severely hampered due to sensitivity issues (Jarrett et al. 2013).

Cluver et al. (2017) gives the SFR correlation with WISE luminosity. This equation was a linear fit to SFR and total infrared luminosity for galaxies from SINGS and KINGFISH using Kroupa's IMF for calculations. The infrared luminosity traces a SFR over last 100 Myr which sensitive to star formation history (Murphy et al. 2011; Hao et al. 2011).

$$\log SFR(M_\odot yr^{-1}) = (0.889 \pm 0.018)\log L_{12\mu m}(L_\odot)$$
$$- (7.76 \pm 0.15)$$
$$\tag{4}$$

The SFRs based on the Salpeter IMF are known to be larger than those based on other IMFs such as Kroupa and Chabrier by a factor of $1.4 - 1.6$ e.g., (Calzetti et al. 2007; Kennicutt et al. 2009). Therefore, it is necessary to take into account these offsets when one compares the calibration results with different IMFs.

2.2 SFR : SED Fitting using MAGPHYS

The Spectral Energy Distribution(SED) of galaxies gives us various information about various physical properties of the galaxy. SED of a galaxy can be theoretically modelled by solving the radiative transfer equations for a known distribution of stars and other components. The SED is obtained by adding contributions from all Simple Stellar Populations in the galaxy (SSPs). In synthesis models a grid of stellar evolutionary track is used to derive the temperature and bolometric luminosity for various stellar masses as a function of time and the integrated flux from the grid is obtained using stellar atmosphere models or spectral libraries. Stellar templates are added with a weighted IMF (Initial Mass Function) to obtain spectra of stellar population of same age. Then these isochrones are added in linear combination to obtain the final spectra with a exponentially parameterized star formation history. Thus the model contains minimum of four parameters: IMF, star formation history, galaxy age and metallicity.

In this study we use publicly available software MAGPHYS (Multi-wavelength Analysis of Galaxy Physical Properties) (da Cunha et al. 2008) for SED fitting. The code uses a stellar population synthesis code by Bruzual & Charlot (2003) to predict the spectral evolution of stellar population. The dust attenuation of stellar spectrum is modelled using the two component model of (Charlot & Fall 2000). The specific intensity of the stellar population at time t with a star formation rate $\psi(t)$ is given as

$$L_\lambda = \int \psi(t')S_\lambda(t', Z)e^{-\tau_\lambda} dt' \tag{2}$$

Here Z is the metallicity of the population and τ_λ is the

Table 1. Tracers : Sample sizes

TRACER	LSBs	STs
GALEX(FUV)	212	158
WISE(W3)	345	549
SED fitting (MAGPHYS)	103	65

opacity of ISM, S_λ is the specific intensity of the simple stellar population(SSP) of age t'. Star formation rate is again modelled as continuous function parameterized by t_{form} and time scale parameter γ. Thus $\psi(t) \propto e^{-\gamma t}$ and random bursts are superimposed to this continuous model.

The optical depth is modelled according Charlot & Fall (2000). The attenuation for the young stars and old stars is different so that

$$\tau_\lambda = \begin{cases} \tau^{BC} + \tau^{ISM} & t' \leqslant 10^7 yr \\ \tau^{ISM} & t' > 10^7 \end{cases} \tag{3}$$

The spectral energy distribution of the power reradiated by dust in the stellar birth clouds is computed as the sum of three components: polycylic aromatic hydrocarbons (PAHs); mid-infrared continuum characterizing the emission from hot grains and grains in thermal equilibrium with adjustable temperature(da Cunha et al. 2008).

3 SAMPLE

We have chosen the LSBs sample from the near IR catalogue of LSBs of Monnier Ragaigne, D. et al. (2003). The STs sample was chosen from Karachentsev et al. (2003). This was cross matched with the catalogue of Bianchi et al. (2017) to obtain the GALEX FUV and NUV magnitudes of our sample LSBs and STs. Similarly, we cross match the catalogue of Monnier Ragaigne, D. et al. (2003) and Karachentsev et al. (2003) with Cutri & et al. (2012) to obtain the WISE 12μ data for our sample galaxies. Only those galaxies were chosen whose distances were available in the NED database as was required for the conversion of magnitude to luminosity. For SED fitting using MAGPHYS, we combine GALEX (NUV, FUV), SDSS (u,g,r,i,z) and NIR (J,H,Ks) photometric data. The photometric redshift was obtained from NED database. For the sample used in MAGPHYS, the asymptotic rotational velocity V_{rot} spans a range of 30 - 252 for STs and 18 - 299 for LSBs. The absolute magnitude M_r has a range of $-21 < M_r < -7$ for STs and $-21 < M_r < -4$ for LSBs in the same sample. Redshift for these galaxies were obtained from NED extra-galactic database. The error in the photometric data were obtained from the respective catalogues and flux calibration was done accordingly. We use Schlegel et al. (1998) for Galactic extinction correction for the GALEX and optical magnitudes. A cross match between Monnier Ragaigne, D. et al. (2003) and Karachentsev et al. (2003) gives zero overlap within 2 ′ radius, indicating that our sample does not have LSBs which are also STs. Then those galaxies which gave $\chi^2 > 5$ in SED fitting were rejected. The sample sizes are summarized in Table 1.

Table 2. Results: SFR of STs and LSBs

Physical parameters	Median value	
	LSBs	STs
SFR - GALEX(FUV)$(M_\odot yr^{-1})$	0.223	0.057
SFR - WISE(W3)$(M_\odot yr^{-1})$	0.471	0.17
SFR - SED fitting(MAGPHYS)$(M_\odot yr^{-1})$	0.616	0.357
No of bursts after tform	1	1
tform(Gyr)	7.5	8.7
star formation time scale$(\gamma(Gyr^{-1}))$	0.17	0.21

4 RESULTS

4.1 SFR : GALEX FUV and WISE NIR (W3)

In Figure 1, we study the distribution of SFR as estimated from FUV magnitudes from GALEX for both STs [red] and LSBs [green]. We find the median SFR is 0.057 $M_\odot yr^{-1}$ for STs and 0.223 $M_\odot yr^{-1}$ for LSBs, and hence our estimated median SFR for STs is almost an order of magnitude smaller than that of the LSBs in general. This may be attributed to dust extinction due to edge-on geometry of the STs, the latter being prone to dust extinction and the Galex FUV magnitudes for our sample galaxies were not corrected for internal dust extinction. The error bar, obtained by propagating the uncertainties in the magnitudes, is only ~ 0.01 M$_\odot yr^{-1}$. However, as far as our estimated SFR for LSBs is in compliance with the study of Wyder et al. (2009), who analysed star formation in a sample of 19 LSBs from de Blok et al. (1995), with asymptotic rotational velocity V_{rot} ranging between 29 - 214 km/s and r band magnitude M_r between $-13 > M_r > -23$, thus spanning galaxy dynamical masses from dwarfs to giants. Their results indicated SFRs in the range of 0.001 to 3.002 $M \odot yr^{-1}$ with 0.27 $M \odot yr^{-1}$ as median where the lowest and highest star formation rate corresponds to a dwarf Irregular (dI) and a giant LSB (GLSB) respectively. Further Karachentseva et al. (2020) used GALEX FUV luminosity to determine the SFR for 181 nealy face-on thin spiral galaxies (log(a/b) < 0.05) and found the median log(sSFR) -10.40 dex yr^{-1} for Sd galaxies. We note the SFR estimate from FUV is more reliable as the calibration between SFR and UV luminosity was not done considering the entire range of NUV(1750-2800) Å) (Roychowdhury et al. 2009)

Source of UV radiation in LSBs and STs:
Figure 2 shows the NUV-r color magnitude diagram of the LSBs and STs in our study with sample used in Wyder et al. (2009). They have little UV emission from older stars $(M_{NUV} - M_r > 4)$. UV luminosity is an indicator of the recent SFR and the r-band luminosity is traces the total stellar mass, so (NUV-r) color is representative of the SFR divided by the stellar mass M_{star}(sSFR), and hence the average age of the stars in a galaxy (Salim et al. 2005). However, the dust attenuation makes the relation between (NUV-r) color and SFR/M_{star} complicated.

Figure 3 (Left) shows the distribtuion of SFR estiamted from WISE luminosity for sample of STs and LSBs. The median SFR is 0.471 $M_\odot/yr$) for STs and 0.17 $M_\odot/yr$) for LSBs. We have quoted the maximum value of the Equation (4) for our sample. Surprisingly STs show a higher SFR than LSBs which may be because of less sensitivity of WISE magnitudes to dust extinction.
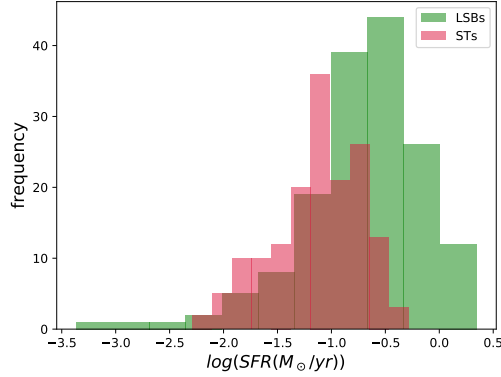
Figure 1. The above figure shows the distribution of star formation rate(SFR) estimated from GALEX(FUV). The green bars are LSBs and red bars are the STs.
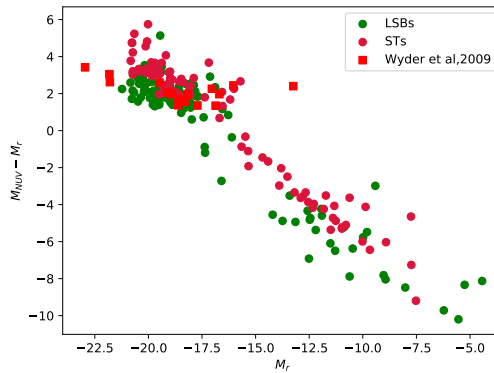

Figure 2. The figure shows the color magnitude diagram for sample used for MAGPHYS. The green circles correspond to LSBs and red ones to STs. The red squares indicates the LSBs from study of Wyder et al.(2009)

4.2 SFR : SED Fitting (MAGPHYS)

Figure 3 (Right) shows the histogram of SFR obtained from MAGPHYS. The red rectangles correspond to STs and green rectangles are for LSBs. The median of SFR from MAGPHYS is 0.616 $M_\odot yr^{-1}$ for LSBs and 0.357 $M_\odot yr^{-1}$ for STs, both of which are one to two orders of magnitude less than the SFR for SINGS galaxies (Spitzer Infrared Nearby Galaxies Survey (da Cunha et al. 2008). MAGPHYS gives us an higher SFR compared to other two SFR values from WISE and GALEX. We estimated the SFR for 45 LSBs and 39 STs including WISE magnitudes, the median of SFR increases to 0.71 and 0.75 respectively. This also increases the median of the dust mass obtained from SED fitting for both the samples.

As shown in Figure 4 (Left), interestingly, most of the galaxies in both samples lie in the star forming region with $log(sSFR) > -10.8$ in the $sSFR - M_*$ plane (Salim 2014). The median of the sSFR distribution is -10.38 and -9.87 for STs and LSBs respectively which shows these are star forming galaxies. Further Karachentseva et al. (2020) used GALEX FUV luminosity to determine the SFR for 181 nealy face-on thin spiral galaxies (log(a/b) < 0.05) and found the median log(sSFR) -10.40 dex yr^{-1} for Sd galaxies. This complies with the $sSFR$ of our sample STGs and LSBs. In Fig-

ure 4 (Right), superimposed on the Kennicutt-Schmidt (K-S) law for the ordinary galaxies are the SFRs of LSBs from Wyder et al. (2009) and the SFRs of dIrrs from Roychowdhury et al. (2009). We note, on an equal footing with dIrrs, the LSBs have a lower SFR compared to ordinary galaxies. We note above that the K-S relation fails on scales of molecular clouds (80 pc). The connection between local and global star formation may be resolved by considering the kinematics of the galaxy. For example, Aouad et al. (2020) shows there is a strong correlation between the Oorts constants and normalised star formation density for 17 nearby spiral galaxies.

The distribution of the random number of bursts after t_{form} (See §4) is shown in Figure 5 (Left), the respective median values both superthins and LSBs being 1, indicating bursts do not play a significant role in modelling the star formation history of LSBs in general. The distribution of star formation time scale parameter Gyr^{-1} (See §4) is presented in Figure 5 (Right). The γ in Gyr^{-1} is distributed between 0.01 and 0.8. The median values for superthins and LSBs are 0.27 Gyr^{-1} and 0.169 Gyr^{-1}. In comparison, $\gamma = 2$ for an elliptical, $\gamma = 0.25$ for an early type and 0.5 for a late type spiral galaxy da Cunha et al. (2008).$\gamma \sim 0$ implies star formation rate was constant along the star formation history of
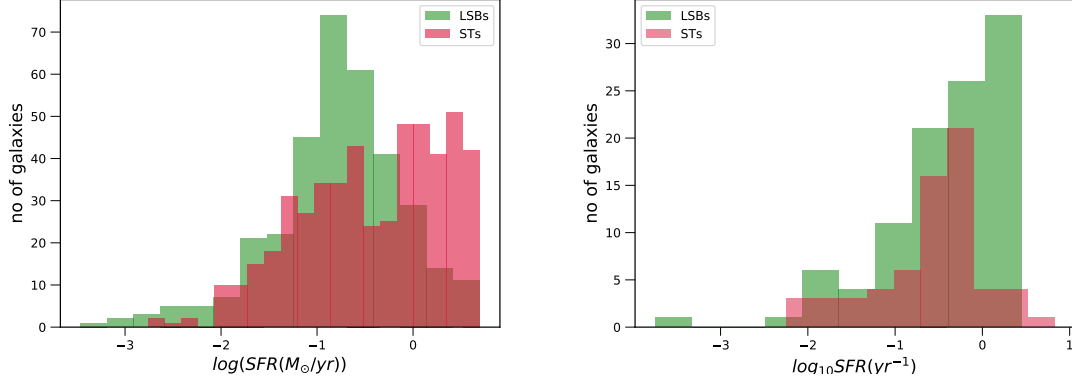
Figure 3. The figure on left shows histogram of SFR estimates for STs and LSBs from WISE (W3) magnitudes. The figure on right shows SFR distribution of LSBs and STs from MAGPHYS. The pink rectangles denote the STs and green rectangles the LSBs in both the plots.
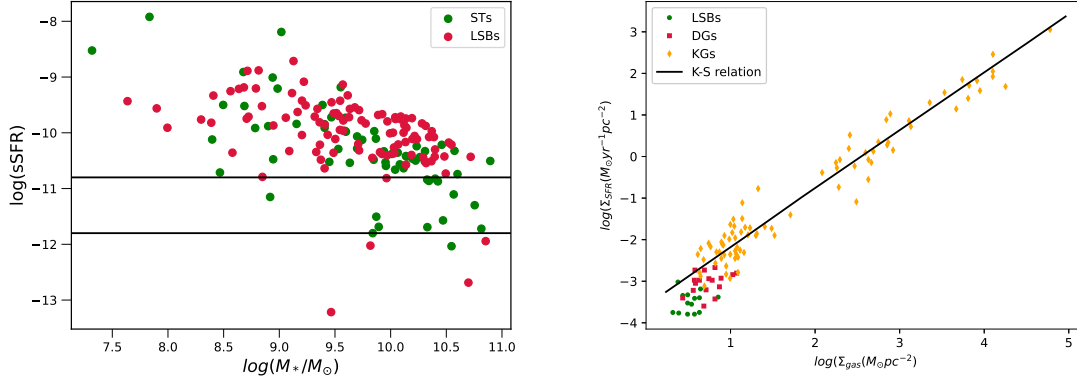
Figure 4. The figure on left shows the scatter plot of log(sSFR) and log(M_*) for STs and LSBs from MAGPHYS. The figure on the right panel shows the Kennicutt-Schmidt relation for galaxies of different morphological types. The green circles are LSB sample from de Blok et al.(1995). The red squares are faint dwarf galaxies from Roychowdhury et al.(2009). The orange diamonds are sample from Kennicutt (1998). The black solid line is the Kennicutt-Schmidt relation for normal star forming galaxies.

the galaxy. Among our sample STs and LSBs, most of the galaxies have $\gamma < 0.5$ which implies these galaxies have star formation histories corresponding to late type or early type spiral galaxies. The minimal number of bursts as well as the low star formation time scale parameter required in modelling star formation history indicates constant star formation rates in these galaxies. This is in compliance with the same order of magnitude of the values of average SFR calculated over the last 0.1 Gyr and 2 Grs respectively (0.357 vs 0.657 $M_\odot yr^{-1}$ for LSBs and 0.616 versus 0.51 $M_\odot yr^{-1}$ for superthins). Figure 6 shows the scatter diagram of $log(SFR(M_\odot yr^{-1}))$ and $log(M_*(M_\odot))$. The solid line represents the Equation (3) de los Reyes et al. (2015).

galaxy in poor in dust content as are the LSBs in general. The dust emission is not well constrained as we haven't included the photometric data beyond $3\mu m$. Figure 7 shows the histogram plot of M_{dust} in these galaxies. There is no significant difference for both STs and LSBs in the modes of their distributions of M_{dust}. The median values for $log(M_{dust}/M_\odot)$ is 7.03 and 6.81 for STs and LSBs respectively. Bogdan (2019) estimated the dust mass for 18 nearby spiral galaxies from KINGFISH survey. The median of $log(M_{dust}/M_\odot)$ for this sample is 7.25, which is slightly greater than median value for our sample of STS and LSBs. da Cunha et.al. (2010) estimated a correlation between SFR and M_{dust} for 3258 galaxies using photometric data from GALEX, 2MASS and IRAS.

5 DISCUSSION

How dusty are the superthins and the LSBs :

From their study of the observed colour gradient in a prototypical superthin galaxy UGC7321, Matthews et al. (1999b) and Matthews & Wood (2001) concluded that the above

Figure 8 shows the scatter plot of SFR and dust masss of our sample STs and LSBs over-plotted on the above correlation. Both sample of galaxies closely follow the above correlation relation.
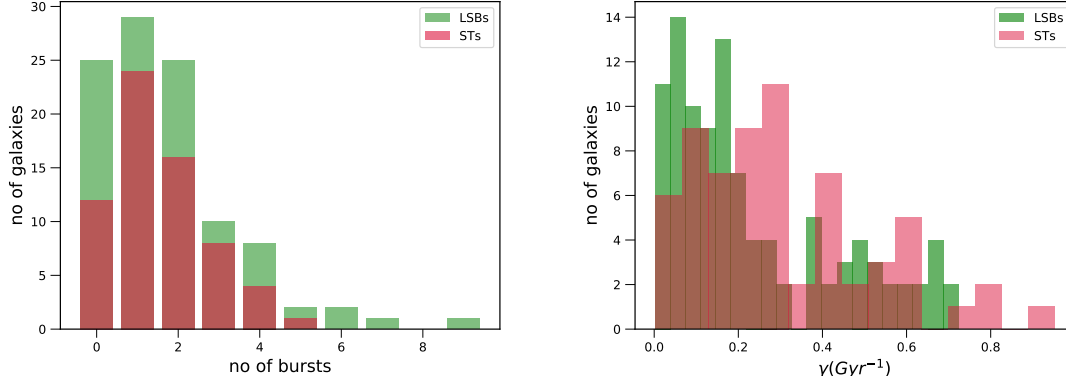
Figure 5. The left figure shows the distribution of number of bursts after t_{form} used in modelling star formation history in MAGPHYS. The red bars shows of number of bursts used in STs sample and the number of bursts used in LSBs. The figure on right is the distribution of timescale of star formation γ in Gyr^{-1}.
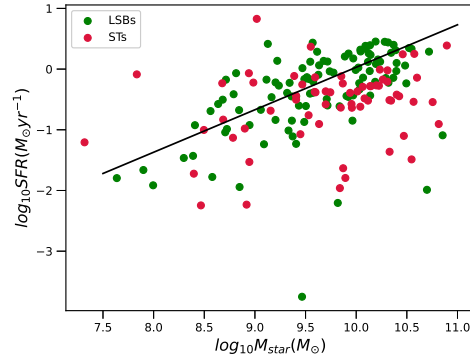
Figure 6. The figure above shows the log(SFR) and $log(M_*)$ scatter plot. The pink dots are STs used for MAGPHYS analysis and green circles are LSBs.
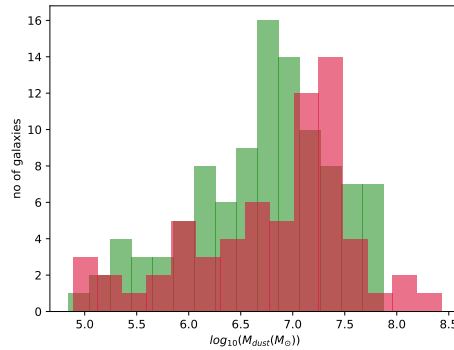
Figure 7. The above figure shows the distribution of dust mass for both LSBs and STs from MAGPHYS. The green rectangles is for LSBs and red rectangle is for STs.

6 CONCLUSIONS

In this work we use luminosity SFR correlations and SED fitting for studying a sample of LSBs and STs. If thickness correction was negligible for STs we could expect a lower value for stability parameter and a higher SFR which can be shown using Jog (1996). We get median SFR of 0.057 $M_\odot/yr$ and 0.223 $M_\odot/yr$ for STs ans LSBs. FUV luminosity predicts a lower SFR for both STs and LSBs compared to other samples. This could be due to the sensitivity of UV
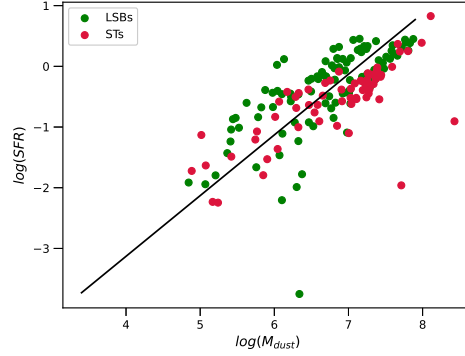
Figure 8. The above figure shows the scatter plot of dust mass and SFR for both LSBs and STs from MAGPHYS. The green circles are LSBs and red circles are STs.

to dust or lower disk thickness of ST sample. SFR is dynamically linked to the local stability parameter. We get a SFR 0.47 $M_\odot/yr$ and 0.17 $M_\odot/yr$ for STs and LSBs from WISE luminosity. The WISE luminosity is less prone to dust extinction and gives a comparable SFR values for STs and LSB sample. SED fitting predicts a SFR value closer to what we obtained from WISE luminosity. The LSBs and STs are evolves slowly like typical disk like galaxies as shown by star formation time scale parameter($gamma \sim 0.1 Gyr^{-1}$). They have similar sSFR compared to HSBs and can be seen among star forming galaxies in sSFR M_{star} scatter diagram. The dust mass is not well constrained as we don't take the dust emission in to account. In SED fitting they follow the same correlation of dust mass with SFR for normal star forming galaxies.

7 DATA AVAILABILITY

We obtained the data from the catalog Monnier Ragaigne, D. et al. (2003), for LSBs and Karachentsev et al. (2003), for STs using Vizier catalogue access tool. A python package ASTROQUERY was used to obtain the photometry data in all bands. Distances to the galaxies were obtained using the NASA/IPAC Extragalactic Database (NED).

8 ACKNOWLEDGEMENTS

REFERENCES

Adami C., et al., 2006, Astronomy & Astrophysics, 459, 679–692
Aouad C. J., James P. A., Chilingarian I. V., 2020, Monthly Notices of the Royal Astronomical Society, 496, 5211
Astropy Collaboration et al., 2018, aj, 156, 123
Bell E. F., Bower R. G., de Jong R. S., Hereld M., Rauscher B. J., 1999, Monthly Notices of the Royal Astronomical Society, 302, L55
Bell E. F., Barnaby D., Bower R. G., de Jong R. S., Harper D. A., Hereld M., Loewenstein R. F., Rauscher B. J., 2000, Monthly Notices of the Royal Astronomical Society, 312, 470
Bianchi L., 2011, Ap&SS, 335, 51
Bianchi L., Shiao B., Thilker D., 2017, The Astrophysical Journal Supplement Series, 230, 24
Bothun G., Impey C., McGaugh S., 1997, PASP, 109, 745
Bradley L., et al., 2020, astropy/photutils: 1.0.0, doi:10.5281/zenodo.4044744, https://doi.org/10.5281/zenodo.4044744
Bruzual G., Charlot S., 2003, MNRAS, 344, 1000
Calzetti D., et al., 2007, The Astrophysical Journal, 666, 870–895
Charlot S., Fall S. M., 2000, ApJ, 539, 718
Cluver M. E., Jarrett T. H., Dale D. A., Smith J.-D. T., August T., Brown M. J. I., 2017, The Astrophysical Journal, 850, 68
Courteau S., 1996, ApJS, 103, 363
Cutri R. M., et al. 2012, VizieR Online Data Catalog, p. II/311
Ginsburg A., et al., 2019, The Astronomical Journal, 157, 98
Hao C.-N., Kennicutt R. C., Johnson B. D., Calzetti D., Dale D. A., Moustakas J., 2011, ApJ, 741, 124
Jarrett T. H., et al., 2013, AJ, 145, 6
Jog C. J., 1996, MNRAS, 278, 209
Karachentsev I., Karachentseva V., Kudrya Y. N., Sharina M., Parnovsky S., 2003, arXiv preprint astro-ph/0305566
Karachentseva V. E., Karachentsev I. D., Kashibadze O. G., 2020, Astrophysics, 63, 151–165
Kennicutt Robert C. J., 1998, ApJ, 498, 541
Kennicutt R. C., et al., 2009, The Astrophysical Journal, 703, 1672–1695

Lee J. C., Kennicutt Robert C. J., Funes S. J. J. G., Sakai S., Akiyama S., 2009, ApJ, 692, 1305

Lei F.-J., Wu H., Zhu Y.-N., Du W., He M., Jin J.-J., Zhao P.-S., Zhang B.-Q., 2019, The Astrophysical Journal Supplement Series, 242, 11

Matthews L. D., Wood K., 2001, The Astrophysical Journal, 548, 150–171

Matthews L. D., van Driel W., Gallagher J. S., 1999a, arXiv e-prints, pp astro–ph/9911022

Matthews L. D., Gallagher J. S. I., van Driel W., 1999b, AJ, 118, 2751

McGaugh S. S., 1994, Nature, 367, 538

McGaugh S. S., Bothun G. D., 1994, AJ, 107, 530

Monnier Ragaigne, D. van Driel, W. O'Neil, K. Schneider, S. E. Balkowski, C. Jarrett, T. H. 2003, A&A, 408, 67

Murphy E. J., et al., 2011, ApJ, 737, 67

O'Neil K., Minchin R., Momjian E., 2008, AIP Conference Proceedings

Roychowdhury S., Chengalur J. N., Begum A., Karachentsev I. D., 2009, Monthly Notices of the Royal Astronomical Society, 397, 1435–1453

Salim S., 2014, Serbian Astronomical Journal, p. 1–14

Salim S., et al., 2005, The Astrophysical Journal, 619, L39

Schlegel D. J., Finkbeiner D. P., Davis M., 1998, ApJ, 500, 525

Schombert J. M., McGaugh S. S., Eder J. A., 2001, AJ, 121, 2420

Takeuchi T. T., Buat V., Iglesias-Páramo J., Boselli A., Burgarella D., 2005, A&A, 432, 423

Worthey G., 1994, ApJS, 95, 107

Wyder T. K., et al., 2009, The Astrophysical Journal, 696, 1834–1853

Zackrisson E., Bergvall N., Östlin G., 2005, A&A, 435, 29

da Cunha E., Charlot S., Elbaz D., 2008, MNRAS, 388, 1595

de Blok W. J. G., van der Hulst J. M., Bothun G. D., 1995, Monthly Notices of the Royal Astronomical Society, 274, 235

de los Reyes M. A., et al., 2015, AJ, 149, 79

van den Hoek L. B., de Blok W. J. G., van der Hulst J. M., de Jong T., 2000, A&A, 357, 397

van der Hulst J. M., Deblok W. J. G., McGaugh S. S., Bothun G. D., 1993, in Shull J. M., Thronson H. A., eds, Evolution of Galaxies and their Environment. pp 92–93

Table 1. MAGPHYS input for LSBs

id	FUV(Jy)	NUV(Jy)	SDSS u(Jy)	SDSS g(Jy)	SDSS r(Jy)	SDSS i(Jy)	SDSS z(Jy)	J(Jy)	H(Jy)	Ks(Jy)
1048	$6.3E-07$	$9.0E-07$	$1.3E-06$	$2.5E-06$	$2.9E-06$	$3.3E-06$	$3.7E-06$	$1.3E-06$	$1.6E-06$	$5.5E-08$
1084	$4.6E-08$	$5.1E-08$	$6.6E-08$	$1.3E-07$	$1.7E-07$	$2.0E-07$	$2.3E-07$	$7.1E-08$	$5.7E-08$	$2.1E-07$
1141	$1.6E-06$	$2.1E-06$	$5.7E-06$	$1.6E-05$	$2.5E-05$	$3.0E-05$	$3.5E-05$	$8.4E-06$	$2.8E-05$	$1.4E-05$
1010	$5.5E-07$	$7.1E-07$	$1.5E-06$	$4.9E-06$	$8.3E-06$	$1.1E-05$	$1.4E-05$	$4.7E-06$	$2.3E-06$	$3.0E-08$
1025	$1.1E-07$	$1.5E-07$	$2.7E-07$	$8.1E-07$	$1.4E-06$	$2.0E-06$	$2.6E-06$	$9.9E-07$	$6.1E-07$	$7.9E-07$
1085	$2.5E-07$	$3.0E-07$	$5.0E-07$	$1.2E-06$	$1.7E-06$	$2.0E-06$	$2.3E-06$	$1.1E-06$	$3.5E-07$	$9.2E-07$
1093	$1.7E-07$	$2.8E-07$	$6.3E-07$	$1.6E-06$	$1.8E-06$	$2.1E-06$	$2.3E-06$	$1.7E-06$	$1.6E-06$	$1.0E-06$
1013	$8.8E-07$	$1.1E-06$	$1.8E-06$	$4.5E-06$	$6.2E-06$	$7.5E-06$	$8.8E-06$	$1.2E-06$	$4.4E-06$	$1.0E-06$
1039	$3.2E-06$	$3.3E-06$	$4.1E-06$	$9.2E-06$	$1.4E-05$	$1.7E-05$	$2.2E-05$	$2.1E-06$	$5.4E-06$	$9.8E-06$
1181	$4.5E-06$	$6.0E-06$	$8.9E-06$	$2.0E-05$	$2.9E-05$	$3.6E-05$	$4.4E-05$	$1.9E-06$	$1.1E-05$	$3.7E-05$
1094	$1.5E-08$	$2.5E-08$	$7.3E-08$	$2.2E-07$	$3.4E-07$	$4.4E-07$	$5.2E-07$	$2.0E-07$	$3.1E-07$	$3.1E-07$
1142	$4.6E-07$	$8.6E-07$	$2.0E-06$	$5.8E-06$	$9.1E-06$	$1.2E-05$	$1.5E-05$	$8.0E-06$	$7.2E-06$	$1.6E-06$
1071	$1.8E-07$	$4.2E-07$	$1.4E-06$	$5.2E-06$	$9.5E-06$	$1.3E-05$	$1.8E-05$	$7.2E-06$	$3.8E-07$	$6.4E-06$
1133	$2.6E-08$	$3.0E-08$	$6.6E-08$	$2.3E-07$	$4.6E-07$	$6.4E-07$	$8.5E-07$	$3.3E-07$	$3.2E-07$	$4.7E-07$
1057	$1.1E-07$	$2.4E-07$	$8.6E-07$	$3.1E-06$	$5.7E-06$	$7.9E-06$	$1.0E-05$	$2.6E-07$	$6.1E-06$	$5.4E-06$
1097	$4.2E-07$	$7.1E-07$	$2.0E-06$	$7.2E-06$	$1.4E-05$	$2.0E-05$	$2.7E-05$	$1.7E-06$	$3.9E-06$	$9.8E-06$
1116	$6.4E-07$	$7.8E-07$	$1.1E-06$	$2.5E-06$	$3.6E-06$	$4.5E-06$	$5.6E-06$	$3.0E-06$	$3.8E-07$	$3.2E-06$
1083	$1.8E-07$	$2.7E-07$	$4.5E-07$	$9.5E-07$	$1.3E-06$	$1.6E-06$	$1.9E-06$	$1.3E-06$	$2.4E-07$	$1.1E-06$
1179	$1.6E-07$	$2.9E-07$	$6.4E-07$	$1.7E-06$	$2.7E-06$	$3.6E-06$	$4.5E-06$	$2.9E-07$	$3.4E-06$	$4.0E-06$
1155	$1.4E-07$	$3.2E-07$	$9.7E-07$	$3.1E-06$	$5.4E-06$	$7.4E-06$	$9.9E-06$	$3.7E-06$	$1.2E-07$	$2.0E-06$
1098	$1.0E-06$	$1.5E-06$	$3.7E-06$	$1.2E-05$	$2.2E-05$	$3.0E-05$	$4.0E-05$	$4.7E-06$	$2.4E-05$	$1.4E-05$
1110	$9.3E-08$	$1.2E-07$	$2.3E-07$	$6.6E-07$	$1.1E-06$	$1.5E-06$	$2.0E-06$	$8.3E-07$	$7.9E-07$	$8.3E-07$
1178	$2.4E-06$	$2.9E-06$	$4.5E-06$	$1.2E-05$	$1.9E-05$	$2.4E-05$	$3.1E-05$	$8.1E-06$	$1.4E-05$	$2.1E-05$
1143	$4.6E-07$	$5.4E-07$	$7.5E-07$	$1.6E-06$	$2.2E-06$	$2.7E-06$	$3.2E-06$	$1.5E-06$	$1.8E-06$	$6.0E-07$
1024	$1.5E-06$	$2.5E-06$	$4.2E-06$	$1.0E-05$	$1.5E-05$	$2.0E-05$	$2.5E-05$	$4.1E-06$	$1.5E-05$	$1.7E-05$
1159	$3.0E-07$	$6.5E-07$	$1.9E-06$	$6.6E-06$	$1.2E-05$	$1.6E-05$	$2.2E-05$	$9.1E-06$	$1.2E-05$	$1.7E-05$
1101	$5.5E-08$	$7.2E-08$	$1.2E-07$	$2.7E-07$	$3.9E-07$	$4.9E-07$	$5.9E-07$	$3.2E-07$	$9.1E-08$	$7.4E-08$
1050	$1.7E-06$	$2.8E-06$	$7.4E-06$	$2.3E-05$	$3.9E-05$	$5.0E-05$	$6.3E-05$	$1.4E-05$	$1.7E-05$	$3.7E-05$
1162	$4.4E-07$	$7.0E-07$	$2.2E-06$	$7.2E-06$	$1.3E-05$	$1.7E-05$	$2.0E-05$	$8.4E-06$	$4.3E-06$	$1.2E-05$
1038	$4.8E-07$	$6.5E-07$	$8.4E-07$	$2.0E-06$	$3.8E-06$	$5.5E-06$	$7.4E-06$	$2.5E-06$	$3.3E-06$	$5.8E-06$
1148	$7.9E-07$	$1.2E-06$	$2.4E-06$	$6.7E-06$	$1.2E-05$	$1.6E-05$	$2.1E-05$	$2.2E-06$	$1.3E-05$	$1.9E-07$
1032	$7.0E-07$	$8.5E-07$	$1.4E-06$	$3.9E-06$	$7.0E-06$	$9.6E-06$	$1.3E-05$	$2.2E-06$	$6.1E-06$	$3.7E-07$
1125	$9.0E-07$	$1.4E-06$	$3.8E-06$	$1.2E-05$	$2.0E-05$	$2.5E-05$	$3.2E-05$	$1.2E-06$	$2.5E-05$	$1.5E-05$
1154	$1.9E-07$	$3.1E-07$	$1.2E-06$	$4.6E-06$	$8.9E-06$	$1.2E-05$	$1.6E-05$	$4.5E-06$	$3.7E-07$	$1.0E-05$
1158	$1.5E-06$	$2.4E-06$	$5.3E-06$	$1.6E-05$	$2.9E-05$	$4.0E-05$	$5.4E-05$	$8.5E-06$	$3.9E-06$	$2.0E-05$
1117	$2.6E-06$	$3.0E-06$	$4.0E-06$	$8.7E-06$	$1.1E-05$	$1.3E-05$	$1.5E-05$	$7.0E-06$	$1.1E-05$	$5.4E-06$
1008	$1.4E-07$	$2.2E-07$	$8.3E-07$	$3.1E-06$	$5.9E-06$	$8.2E-06$	$1.1E-05$	$1.0E-06$	$1.4E-06$	$3.0E-06$
1014	$3.9E-06$	$4.1E-06$	$5.1E-06$	$1.1E-05$	$1.7E-05$	$2.1E-05$	$2.7E-05$	$1.6E-05$	$7.3E-06$	$4.6E-06$
1090	$1.2E-06$	$1.5E-06$	$2.3E-06$	$5.3E-06$	$7.3E-06$	$8.9E-06$	$1.1E-05$	$5.5E-06$	$4.0E-06$	$7.5E-06$
1066	$1.9E-07$	$3.6E-07$	$1.3E-06$	$4.1E-06$	$6.8E-06$	$8.8E-06$	$1.0E-05$	$4.8E-07$	$6.9E-06$	$6.4E-08$
1106	$2.1E-07$	$3.4E-07$	$8.2E-07$	$2.3E-06$	$3.3E-06$	$4.1E-06$	$4.9E-06$	$2.8E-06$	$1.5E-06$	$8.1E-07$
1076	$7.5E-07$	$1.0E-06$	$2.9E-06$	$8.5E-06$	$1.4E-05$	$1.7E-05$	$2.0E-05$	$8.7E-06$	$1.5E-05$	$7.0E-06$
1170	$3.9E-06$	$4.9E-06$	$6.8E-06$	$1.5E-05$	$2.1E-05$	$2.6E-05$	$3.2E-05$	$1.0E-05$	$1.5E-05$	$1.1E-06$
1001	$4.4E-07$	$6.8E-07$	$2.7E-06$	$9.6E-06$	$1.8E-05$	$2.4E-05$	$3.1E-05$	$8.1E-06$	$2.1E-05$	$2.3E-05$
1118	$3.1E-07$	$5.1E-07$	$8.1E-07$	$1.9E-06$	$2.6E-06$	$3.2E-06$	$4.0E-06$	$2.3E-07$	$2.9E-06$	$3.6E-06$
1064	$1.6E-06$	$2.6E-06$	$5.3E-06$	$1.5E-05$	$2.7E-05$	$3.6E-05$	$4.7E-05$	$1.8E-05$	$2.7E-05$	$5.1E-06$
1124	$1.9E-08$	$2.8E-08$	$5.7E-08$	$1.4E-07$	$1.9E-07$	$2.3E-07$	$2.6E-07$	$1.3E-07$	$1.6E-07$	$2.6E-07$
1134	$2.2E-07$	$2.6E-07$	$4.0E-07$	$1.1E-06$	$1.9E-06$	$2.6E-06$	$3.4E-06$	$8.8E-08$	$1.0E-06$	$5.4E-07$
1089	$1.7E-06$	$2.0E-06$	$2.6E-06$	$5.4E-06$	$7.3E-06$	$8.8E-06$	$1.0E-05$	$5.6E-06$	$2.2E-06$	$9.2E-06$
1163	$2.7E-07$	$5.0E-07$	$1.3E-06$	$3.7E-06$	$5.9E-06$	$7.6E-06$	$9.5E-06$	$3.7E-07$	$1.7E-06$	$3.3E-06$
1166	$2.4E-07$	$3.9E-07$	$8.3E-07$	$2.3E-06$	$3.7E-06$	$4.8E-06$	$6.0E-06$	$1.2E-06$	$1.9E-06$	$2.0E-06$
1088	$1.1E-06$	$1.2E-06$	$1.6E-06$	$3.8E-06$	$5.6E-06$	$7.1E-06$	$8.7E-06$	$8.9E-07$	$2.4E-06$	$7.5E-06$
1152	$2.8E-07$	$1.1E-06$	$1.1E-05$	$3.8E-05$	$7.2E-05$	$9.4E-05$	$1.1E-04$	$3.7E-05$	$8.4E-05$	$9.2E-05$
1063	$1.9E-06$	$2.9E-06$	$5.3E-06$	$1.5E-05$	$2.5E-05$	$3.3E-05$	$4.3E-05$	$6.9E-06$	$1.0E-05$	$1.9E-05$
1069	$1.1E-06$	$1.8E-06$	$3.2E-06$	$8.3E-06$	$1.3E-05$	$1.7E-05$	$2.2E-05$	$1.1E-05$	$4.0E-06$	$1.7E-05$
1102	$1.1E-06$	$1.4E-06$	$3.0E-06$	$1.0E-05$	$2.0E-05$	$2.8E-05$	$3.8E-05$	$1.2E-05$	$2.0E-05$	$3.9E-06$
1147	$2.3E-06$	$3.5E-06$	$6.7E-06$	$1.8E-05$	$2.8E-05$	$3.5E-05$	$4.3E-05$	$5.7E-06$	$1.5E-05$	$2.5E-05$
1135	$3.5E-07$	$5.0E-07$	$1.1E-06$	$3.0E-06$	$4.7E-06$	$5.9E-06$	$7.2E-06$	$9.4E-07$	$4.5E-06$	$3.1E-06$
1130	$1.1E-07$	$1.7E-07$	$3.4E-07$	$8.6E-07$	$1.1E-06$	$1.3E-06$	$1.5E-06$	$7.3E-07$	$7.2E-07$	$5.7E-07$
1044	$1.1E-06$	$1.5E-06$	$2.9E-06$	$7.6E-06$	$1.1E-05$	$1.3E-05$	$1.6E-05$	$6.5E-06$	$7.5E-06$	$2.8E-06$
1119	$4.1E-06$	$5.0E-06$	$7.9E-06$	$2.3E-05$	$4.1E-05$	$5.7E-05$	$7.7E-05$	$1.2E-05$	$3.2E-05$	$1.2E-05$
1016	$6.6E-07$	$9.7E-07$	$1.6E-06$	$3.8E-06$	$5.6E-06$	$7.0E-06$	$8.6E-06$	$9.8E-07$	$6.5E-06$	$5.2E-07$
1120	$3.2E-07$	$4.0E-07$	$4.8E-07$	$7.8E-07$	$9.2E-07$	$1.1E-06$	$1.2E-06$	$3.6E-07$	$2.8E-07$	$1.1E-06$
1046	$1.1E-08$	$4.6E-08$	$6.4E-07$	$2.6E-06$	$5.1E-06$	$7.0E-06$	$8.9E-06$	$1.6E-07$	$4.2E-06$	$4.8E-06$

Table 2. MAGPHYS input for STs

id	FUV ^{a}	NUV^b	u^c	g ^{d}	r^e	i ^{f}	z ^{g}	J ^{h}	H ^{i}	Ks ^{j}
1115	$3.5E-07$	$5.7E-07$	$1.5E-06$	$5.3E-06$	$9.9E-06$	$1.4E-05$	$1.8E-05$	$5.4E-06$	$1.2E-05$	$2.3E-07$
1076	$3.6E-07$	$5.4E-07$	$2.0E-06$	$6.4E-06$	$1.1E-05$	$1.4E-05$	$1.7E-05$	$1.8E-07$	$1.1E-05$	$4.1E-08$
1001	$2.9E-07$	$4.4E-07$	$1.1E-06$	$3.5E-06$	$6.2E-06$	$8.4E-06$	$1.1E-05$	$1.1E-06$	$3.0E-06$	$8.8E-07$
1118	$1.7E-07$	$3.5E-07$	$1.6E-06$	$5.4E-06$	$9.7E-06$	$1.3E-05$	$1.5E-05$	$7.7E-07$	$5.2E-06$	$3.9E-07$
1064	$1.4E-06$	$2.3E-06$	$7.2E-06$	$2.1E-05$	$3.4E-05$	$4.1E-05$	$4.7E-05$	$2.4E-05$	$2.7E-05$	$7.3E-06$
1047	$8.8E-08$	$2.0E-07$	$8.4E-07$	$3.1E-06$	$5.7E-06$	$7.9E-06$	$1.0E-05$	$2.2E-06$	$1.8E-07$	$2.1E-06$
1030	$2.0E-07$	$3.5E-07$	$2.6E-06$	$1.1E-05$	$2.3E-05$	$3.3E-05$	$4.3E-05$	$1.1E-05$	$1.5E-05$	$5.3E-06$
1089	$3.7E-07$	$6.3E-07$	$2.0E-06$	$6.2E-06$	$1.0E-05$	$1.3E-05$	$1.5E-05$	$1.2E-06$	$2.1E-06$	$2.0E-07$
1006	$3.3E-08$	$2.8E-07$	$1.7E-06$	$6.9E-06$	$1.1E-05$	$1.4E-05$	$1.8E-05$	$1.5E-06$	$3.0E-06$	$1.2E-06$
1063	$2.5E-07$	$4.6E-07$	$1.7E-06$	$5.5E-06$	$9.7E-06$	$1.3E-05$	$1.6E-05$	$5.5E-06$	$4.0E-06$	$4.4E-06$
1069	$5.7E-07$	$9.7E-07$	$2.3E-06$	$7.6E-06$	$1.4E-05$	$1.9E-05$	$2.6E-05$	$1.1E-05$	$1.1E-05$	$8.0E-06$
1049	$7.8E-07$	$1.5E-06$	$2.8E-06$	$6.7E-06$	$9.2E-06$	$1.1E-05$	$1.4E-05$	$6.2E-07$	$2.5E-06$	$1.6E-07$
1102	$7.2E-07$	$1.3E-06$	$4.2E-06$	$1.4E-05$	$2.1E-05$	$2.6E-05$	$3.2E-05$	$6.7E-06$	$4.6E-06$	$4.9E-06$
1103	$4.0E-07$	$6.2E-07$	$2.2E-06$	$7.3E-06$	$1.3E-05$	$1.7E-05$	$2.0E-05$	$7.8E-06$	$5.7E-06$	$3.3E-06$
1044	$2.6E-07$	$4.4E-07$	$1.1E-06$	$3.7E-06$	$7.5E-06$	$1.1E-05$	$1.5E-05$	$2.3E-06$	$7.5E-06$	$1.9E-07$
1119	$1.5E-08$	$3.5E-08$	$1.8E-07$	$5.5E-07$	$9.1E-07$	$1.1E-06$	$1.3E-06$	$2.9E-07$	$2.8E-07$	$2.7E-07$
1029	$2.1E-07$	$3.2E-07$	$8.4E-07$	$3.0E-06$	$5.7E-06$	$8.1E-06$	$1.1E-05$	$2.4E-06$	$3.9E-06$	$1.1E-06$
1046	$1.8E-07$	$3.7E-07$	$1.3E-06$	$5.1E-06$	$1.0E-05$	$1.5E-05$	$2.0E-05$	$7.7E-06$	$1.2E-05$	$3.7E-06$
1018	$3.0E-07$	$4.7E-07$	$9.4E-07$	$2.5E-06$	$3.2E-06$	$3.7E-06$	$4.3E-06$	$2.1E-06$	$1.6E-06$	$1.7E-07$
1042	$3.4E-07$	$4.4E-07$	$7.7E-07$	$2.3E-06$	$4.2E-06$	$5.7E-06$	$7.5E-06$	$2.6E-06$	$1.5E-06$	$2.4E-06$
1113	$6.1E-08$	$1.6E-07$	$4.8E-07$	$1.5E-06$	$2.6E-06$	$3.8E-06$	$5.2E-06$	$1.6E-06$	$1.6E-07$	$1.5E-06$
1053	$3.6E-07$	$5.3E-07$	$1.3E-06$	$3.7E-06$	$5.9E-06$	$7.4E-06$	$9.1E-06$	$1.5E-06$	$1.4E-06$	$5.3E-07$
1015	$2.3E-07$	$3.7E-07$	$8.4E-07$	$2.7E-06$	$4.4E-06$	$5.8E-06$	$7.4E-06$	$8.0E-07$	$2.8E-06$	$1.6E-07$
1075	$1.9E-08$	$4.2E-08$	$7.9E-07$	$3.7E-06$	$7.8E-06$	$1.1E-05$	$1.5E-05$	$6.9E-06$	$6.9E-06$	$5.7E-06$
1031	$5.4E-07$	$9.4E-07$	$3.2E-06$	$1.1E-05$	$1.9E-05$	$2.5E-05$	$3.1E-05$	$9.4E-06$	$6.5E-06$	$4.7E-06$
1036	$3.3E-07$	$5.2E-07$	$8.7E-07$	$2.0E-06$	$2.4E-06$	$2.7E-06$	$3.0E-06$	$2.7E-07$	$2.2E-06$	$1.1E-07$
1104	$1.8E-07$	$2.5E-07$	$4.3E-07$	$1.0E-06$	$1.4E-06$	$1.6E-06$	$1.9E-06$	$9.0E-08$	$9.1E-07$	$7.8E-08$
1091	$1.1E-07$	$3.1E-07$	$7.5E-07$	$2.1E-06$	$2.8E-06$	$3.3E-06$	$4.0E-06$	$7.3E-07$	$2.6E-06$	$4.6E-07$
1087	$7.4E-08$	$1.1E-07$	$1.1E-06$	$4.4E-06$	$8.8E-06$	$1.2E-05$	$1.5E-05$	$1.9E-07$	$7.7E-06$	$6.9E-08$
1045	$4.2E-07$	$5.3E-07$	$1.1E-06$	$3.3E-06$	$5.5E-06$	$7.2E-06$	$9.3E-06$	$4.1E-06$	$4.6E-06$	$3.5E-06$
1109	$2.3E-07$	$2.7E-07$	$5.7E-07$	$1.6E-06$	$2.2E-06$	$2.6E-06$	$3.0E-06$	$5.1E-07$	$1.8E-06$	$4.2E-08$
1002	$2.7E-07$	$3.6E-07$	$4.7E-07$	$7.5E-07$	$8.0E-07$	$8.2E-07$	$8.4E-07$	$7.4E-07$	$1.1E-07$	$6.7E-08$
1061	$2.1E-07$	$4.1E-07$	$1.2E-06$	$4.1E-06$	$7.3E-06$	$9.9E-06$	$1.3E-05$	$9.1E-07$	$3.4E-06$	$7.3E-07$
1022	$5.4E-09$	$1.4E-08$	$3.1E-08$	$6.6E-08$	$8.1E-08$	$9.9E-08$	$1.3E-07$	$2.7E-08$	$4.1E-08$	$1.7E-08$
1000	$5.1E-08$	$1.9E-07$	$4.9E-07$	$1.1E-06$	$1.6E-06$	$2.0E-06$	$2.4E-06$	$5.0E-07$	$1.2E-06$	$3.7E-07$
1020	$5.7E-07$	$7.1E-07$	$1.2E-06$	$3.7E-06$	$7.0E-06$	$9.8E-06$	$1.3E-05$	$4.2E-06$	$6.5E-06$	$6.4E-07$
1081	$3.8E-07$	$6.1E-07$	$1.5E-06$	$5.0E-06$	$9.6E-06$	$1.4E-05$	$1.8E-05$	$7.4E-06$	$9.3E-06$	$1.9E-06$
1074	$1.9E-07$	$3.6E-07$	$9.4E-07$	$2.8E-06$	$4.4E-06$	$5.7E-06$	$7.3E-06$	$8.0E-08$	$4.2E-06$	$9.9E-10$
1027	$1.4E-07$	$2.9E-07$	$1.8E-06$	$6.8E-06$	$1.4E-05$	$1.9E-05$	$2.4E-05$	$1.2E-05$	$2.5E-06$	$3.0E-06$
1062	$2.3E-08$	$2.8E-07$	$3.0E-06$	$1.2E-05$	$2.5E-05$	$3.6E-05$	$4.6E-05$	$1.8E-05$	$1.6E-05$	$1.5E-05$
1077	$3.3E-07$	$5.6E-07$	$1.2E-06$	$3.9E-06$	$7.4E-06$	$1.1E-05$	$1.5E-05$	$4.4E-06$	$4.8E-06$	$3.3E-06$
1028	$5.2E-07$	$7.4E-07$	$1.2E-06$	$3.2E-06$	$4.6E-06$	$5.7E-06$	$7.1E-06$	$2.2E-06$	$3.1E-06$	$1.8E-06$
1092	$1.6E-07$	$2.2E-07$	$5.1E-07$	$1.5E-06$	$2.4E-06$	$3.0E-06$	$3.7E-06$	$1.8E-06$	$2.8E-06$	$1.5E-06$
1012	$3.6E-07$	$6.5E-07$	$1.9E-06$	$7.5E-06$	$1.7E-05$	$2.5E-05$	$3.5E-05$	$1.0E-05$	$1.9E-05$	$2.3E-06$
1040	$2.9E-07$	$4.9E-07$	$9.9E-07$	$2.5E-06$	$3.1E-06$	$3.6E-06$	$4.2E-06$	$2.8E-06$	$6.8E-07$	$4.6E-07$

^{a} GALEX FUV flux density in units of Jansky

^{b} GALEX NUV flux density in units of Jansky

^{c} SDSS u band flux density in units of Jansky

^{d} SDSS g band flux density in units of Jansky

^{e} SDSS r band flux density in units of Jansky

^{f} i flux density in units of Jansky

^{g} z flux density in units of Jansky

^{h} 2MASS J band flux density in units of Jansky

^{i} 2MASS H flux density in units of Jansky

^{j} 2MASS Ks flux density in units of Jansky

Table 3. MAGPHYS ouptut LSBs

id	$M_{star}(M_\odot)$	sSFR	SFR(0.1 Gyr)	L_{dust}	$M_{dust}(M_\odot)$	$\gamma(Gyr^{-1})$	N bursts	tform
1048	$5.17E+08$	$1.29E-09$	$6.69E-01$	$5.46E+09$	$5.02E+06$	$2.11E-01$	$0.00E+00$	$1.07E+09$
1084	$4.33E+07$	$3.69E-10$	$1.60E-02$	$1.52E+08$	$1.61E+05$	$1.54E-01$	$3.00E+00$	$4.69E+09$
1141	$1.54E+10$	$4.01E-11$	$6.17E-01$	$4.26E+09$	$3.92E+06$	$2.36E-01$	$2.00E+00$	$1.00E+10$
1010	$1.07E+10$	$5.45E-11$	$5.85E-01$	$5.74E+09$	$5.28E+06$	$1.80E-02$	$1.00E+00$	$1.19E+10$
1025	$2.36E+09$	$3.29E-11$	$7.78E-02$	$6.09E+08$	$1.29E+06$	$1.70E-02$	$2.00E+00$	$1.29E+10$
1085	$5.09E+08$	$1.79E-10$	$9.09E-02$	$2.46E+08$	$2.62E+05$	$4.40E-01$	$2.00E+00$	$2.99E+09$
1093	$3.79E+08$	$4.40E-11$	$1.67E-02$	$1.51E+09$	$2.37E+06$	$5.50E-01$	$1.00E+00$	$3.78E+09$
1013	$2.20E+09$	$2.69E-10$	$5.94E-01$	$4.95E+09$	$1.05E+07$	$5.02E-01$	$0.00E+00$	$2.90E+09$
1039	$1.05E+10$	$1.01E-10$	$1.06E+00$	$1.02E+09$	$1.09E+06$	$6.00E-02$	$1.00E+00$	$1.13E+10$
1181	$1.55E+10$	$1.83E-10$	$2.84E+00$	$1.33E+10$	$1.41E+07$	$2.40E-02$	$2.00E+00$	$6.16E+09$
1094	$1.99E+08$	$1.73E-10$	$3.43E-02$	$5.56E+08$	$1.18E+06$	$2.77E-01$	$1.00E+00$	$3.99E+09$
1142	$7.72E+09$	$2.09E-10$	$1.61E+00$	$1.92E+10$	$4.05E+07$	$4.20E-02$	$0.00E+00$	$7.34E+09$
1071	$1.33E+10$	$1.37E-10$	$1.82E+00$	$3.05E+10$	$6.43E+07$	$2.67E-01$	$0.00E+00$	$5.69E+09$
1133	$7.06E+08$	$1.62E-11$	$1.14E-02$	$5.56E+07$	$1.17E+05$	$1.17E-01$	$2.00E+00$	$1.26E+10$
1057	$5.48E+09$	$1.67E-10$	$9.19E-01$	$1.43E+10$	$3.02E+07$	$4.36E-01$	$2.00E+00$	$2.89E+09$
1097	$2.33E+10$	$3.09E-11$	$7.17E-01$	$9.68E+09$	$2.04E+07$	$7.20E-02$	$4.00E+00$	$1.13E+10$
1116	$2.30E+09$	$1.54E-10$	$3.55E-01$	$1.80E+09$	$1.65E+06$	$1.20E-01$	$0.00E+00$	$7.36E+09$
1083	$6.52E+08$	$1.32E-09$	$8.56E-01$	$9.78E+09$	$8.99E+06$	$3.82E-01$	$3.00E+00$	$7.83E+09$
1179	$2.08E+09$	$1.95E-10$	$4.06E-01$	$4.92E+09$	$1.04E+07$	$9.00E-02$	$2.00E+00$	$4.84E+09$
1155	$5.21E+09$	$2.55E-10$	$1.33E+00$	$1.72E+10$	$3.63E+07$	$3.12E-01$	$1.00E+00$	$3.59E+09$
1098	$2.49E+10$	$3.73E-11$	$9.30E-01$	$7.05E+09$	$6.48E+06$	$2.02E-01$	$1.00E+00$	$1.12E+10$
1110	$1.23E+09$	$4.71E-11$	$5.78E-02$	$2.79E+08$	$2.57E+05$	$8.90E-02$	$2.00E+00$	$1.20E+10$
1178	$1.57E+10$	$7.74E-11$	$1.21E+00$	$5.34E+09$	$4.91E+06$	$1.54E-01$	$4.00E+00$	$8.14E+09$
1143	$1.14E+09$	$1.87E-10$	$2.13E-01$	$9.01E+08$	$9.58E+05$	$3.00E-03$	$0.00E+00$	$9.59E+09$
1024	$1.11E+10$	$1.77E-10$	$1.95E+00$	$1.57E+10$	$1.44E+07$	$1.18E-01$	$0.00E+00$	$6.71E+09$
1159	$1.23E+10$	$1.96E-10$	$2.41E+00$	$3.20E+10$	$6.76E+07$	$1.20E-01$	$1.00E+00$	$4.01E+09$
1101	$2.45E+08$	$1.52E-10$	$3.72E-02$	$2.53E+08$	$2.32E+05$	$4.60E-02$	$1.00E+00$	$8.66E+09$
1050	$2.34E+10$	$1.07E-10$	$2.51E+00$	$2.84E+10$	$5.99E+07$	$3.80E-01$	$2.00E+00$	$3.43E+09$
1162	$1.08E+10$	$4.30E-11$	$4.63E-01$	$9.28E+09$	$1.96E+07$	$5.76E-01$	$0.00E+00$	$5.72E+09$
1038	$9.19E+09$	$1.54E-11$	$1.41E-01$	$6.85E+09$	$6.30E+06$	$1.56E-01$	$5.00E+00$	$1.32E+10$
1148	$1.36E+10$	$6.82E-11$	$9.29E-01$	$7.93E+09$	$7.29E+06$	$2.60E-02$	$2.00E+00$	$8.46E+09$
1032	$8.37E+09$	$4.16E-11$	$3.48E-01$	$1.38E+09$	$1.27E+06$	$2.00E-03$	$3.00E+00$	$8.91E+09$
1125	$9.87E+09$	$9.78E-11$	$9.68E-01$	$8.11E+09$	$7.46E+06$	$2.21E-01$	$1.00E+00$	$2.80E+09$
1154	$8.02E+09$	$4.49E-11$	$3.60E-01$	$4.80E+09$	$1.02E+07$	$5.27E-01$	$2.00E+00$	$4.55E+09$
1158	$3.52E+10$	$6.12E-11$	$2.16E+00$	$1.97E+10$	$1.81E+07$	$7.70E-02$	$1.00E+00$	$6.12E+09$
1117	$3.52E+09$	$3.76E-10$	$1.32E+00$	$7.75E+09$	$7.12E+06$	$1.00E-01$	$1.00E+00$	$3.36E+09$
1008	$5.21E+09$	$4.83E-11$	$2.52E-01$	$3.16E+09$	$6.68E+06$	$1.77E-01$	$3.00E+00$	$5.19E+09$
1014	$1.31E+10$	$1.01E-10$	$1.31E+00$	$1.27E+09$	$1.35E+06$	$6.00E-02$	$1.00E+00$	$1.13E+10$
1090	$3.08E+09$	$2.23E-10$	$6.85E-01$	$4.14E+09$	$3.81E+06$	$2.60E-01$	$0.00E+00$	$4.31E+09$
1066	$6.85E+09$	$3.55E-11$	$2.44E-01$	$5.03E+09$	$1.06E+07$	$3.70E-02$	$3.00E+00$	$1.25E+10$
1106	$1.72E+09$	$3.10E-10$	$5.35E-01$	$7.91E+09$	$1.67E+07$	$7.90E-02$	$0.00E+00$	$4.76E+09$
1076	$9.33E+09$	$3.95E-11$	$3.69E-01$	$4.14E+09$	$8.75E+06$	$1.07E-01$	$3.00E+00$	$8.20E+09$
1170	$1.10E+10$	$1.90E-10$	$2.09E+00$	$8.10E+09$	$7.45E+06$	$8.50E-02$	$3.00E+00$	$5.80E+09$
1001	$2.08E+10$	$2.86E-11$	$5.96E-01$	$1.07E+10$	$2.25E+07$	$4.10E-01$	$0.00E+00$	$8.20E+09$
1118	$2.55E+09$	$2.30E-11$	$5.87E-02$	$1.98E+09$	$2.11E+06$	$5.04E-01$	$3.00E+00$	$1.30E+10$
1064	$3.33E+10$	$6.67E-11$	$2.22E+00$	$2.08E+10$	$3.94E+07$	$4.70E-02$	$4.00E+00$	$1.19E+10$
1124	$7.92E+07$	$2.74E-10$	$2.17E-02$	$2.70E+08$	$5.71E+05$	$6.10E-02$	$1.00E+00$	$4.50E+09$
1134	$2.15E+09$	$4.53E-11$	$9.73E-02$	$3.63E+08$	$3.34E+05$	$1.43E-01$	$1.00E+00$	$8.08E+09$
1089	$2.95E+09$	$3.52E-10$	$1.04E+00$	$6.51E+09$	$5.99E+06$	$6.33E-01$	$1.00E+00$	$3.95E+09$
1163	$3.26E+09$	$2.25E-10$	$7.36E-01$	$8.44E+09$	$1.78E+07$	$1.70E-01$	$2.00E+00$	$2.44E+09$
1166	$2.56E+09$	$1.40E-10$	$3.58E-01$	$3.96E+09$	$8.37E+06$	$4.68E-01$	$1.00E+00$	$4.10E+09$
1088	$3.74E+09$	$1.09E-10$	$4.07E-01$	$8.20E+08$	$7.54E+05$	$1.64E-01$	$0.00E+00$	$8.12E+09$
1152	$7.14E+10$	$1.14E-12$	$8.11E-02$	$6.12E+09$	$9.57E+06$	$6.68E-01$	$1.00E+00$	$9.35E+09$
1063	$2.21E+10$	$8.39E-11$	$1.86E+00$	$1.45E+10$	$1.34E+07$	$3.23E-01$	$1.00E+00$	$5.88E+09$
1069	$8.40E+09$	$2.16E-10$	$1.80E+00$	$1.81E+10$	$3.81E+07$	$5.37E-01$	$0.00E+00$	$3.15E+09$
1102	$3.12E+10$	$1.86E-11$	$5.82E-01$	$3.14E+09$	$2.89E+06$	$2.17E-01$	$2.00E+00$	$1.19E+10$
1147	$2.06E+10$	$1.33E-10$	$2.75E+00$	$2.74E+10$	$5.80E+07$	$1.43E-01$	$0.00E+00$	$7.62E+09$
1135	$3.18E+09$	$7.74E-11$	$2.46E-01$	$2.32E+09$	$4.90E+06$	$2.43E-01$	$4.00E+00$	$6.39E+09$
1130	$3.65E+08$	$5.58E-10$	$2.03E-01$	$2.77E+09$	$5.85E+06$	$1.73E-01$	$0.00E+00$	$2.47E+09$
1044	$5.97E+09$	$1.47E-10$	$8.74E-01$	$1.05E+10$	$2.22E+07$	$5.10E-02$	$2.00E+00$	$7.68E+09$
1119	$5.23E+10$	$3.71E-11$	$1.94E+00$	$6.81E+09$	$6.26E+06$	$1.80E-01$	$2.00E+00$	$1.04E+10$
1016	$3.42E+09$	$2.00E-10$	$6.86E-01$	$5.39E+09$	$4.95E+06$	$6.90E-02$	$1.00E+00$	$6.32E+09$
1120	$4.34E+08$	$6.13E-10$	$2.66E-01$	$1.81E+09$	$1.67E+06$	$5.04E-01$	$2.00E+00$	$8.41E+09$
1046	$6.58E+09$	$9.47E-13$	$6.24E-03$	$8.10E+08$	$1.27E+06$	$6.10E-01$	$2.00E+00$	$1.12E+10$

Table 4. MAGPHYS ouptut STs

id [a]	$M_{star}(M_\odot)$ [b]	sSFR [c]	SFR(0.1 Gyr) [d]	L_{dust} [e]	$M_{dust}(M_\odot)$ [f]	$\gamma(Gyr^{-1})$ [g]	N bursts [h]	tform [i]
1115	$1.58E+10$	$3.42E-11$	$5.39E-01$	$7.80E+09$	$1.65E+07$	$1.19E-01$	$4.00E+00$	$1.26E+10$
1076	$8.99E+09$	$2.96E-11$	$2.66E-01$	$3.88E+09$	$8.19E+06$	$3.01E-01$	$1.00E+00$	$7.26E+09$
1001	$7.37E+09$	$7.85E-11$	$5.79E-01$	$6.91E+09$	$1.46E+07$	$1.16E-01$	$3.00E+00$	$1.03E+10$
1118	$1.10E+10$	$2.18E-11$	$2.40E-01$	$6.51E+09$	$1.10E+07$	$3.96E-01$	$1.00E+00$	$9.05E+09$
1064	$2.51E+10$	$1.51E-11$	$3.79E-01$	$1.62E+09$	$1.49E+06$	$3.10E-01$	$4.00E+00$	$1.08E+10$
1047	$5.00E+09$	$8.61E-11$	$4.30E-01$	$8.01E+09$	$1.69E+07$	$2.01E-01$	$2.00E+00$	$3.94E+09$
1030	$2.21E+10$	$1.37E-11$	$3.02E-01$	$6.02E+09$	$1.27E+07$	$5.07E-01$	$2.00E+00$	$6.14E+09$
1089	$8.70E+09$	$4.66E-11$	$4.06E-01$	$7.39E+09$	$1.56E+07$	$3.03E-01$	$1.00E+00$	$8.41E+09$
1006	$6.90E+09$	$1.59E-12$	$1.09E-02$	$7.85E+09$	$5.16E+07$	$5.87E-01$	$2.00E+00$	$9.70E+09$
1063	$1.16E+10$	$4.41E-11$	$5.11E-01$	$1.03E+10$	$2.18E+07$	$2.46E-01$	$1.00E+00$	$9.84E+09$
1069	$2.04E+10$	$4.69E-11$	$9.54E-01$	$1.16E+10$	$2.45E+07$	$2.57E-01$	$1.00E+00$	$9.37E+09$
1049	$3.56E+09$	$6.57E-10$	$2.34E+00$	$2.44E+10$	$4.63E+07$	$1.98E-01$	$0.00E+00$	$2.03E+09$
1102	$5.00E+09$	$5.24E-11$	$2.62E-01$	$1.26E+09$	$1.16E+06$	$2.90E-01$	$1.00E+00$	$4.14E+09$
1103	$1.31E+10$	$2.31E-11$	$3.02E-01$	$5.06E+09$	$1.07E+07$	$3.33E-01$	$1.00E+00$	$1.01E+10$
1044	$1.37E+10$	$3.82E-11$	$5.23E-01$	$8.49E+09$	$1.79E+07$	$1.50E-02$	$4.00E+00$	$9.62E+09$
1119	$8.28E+08$	$7.07E-12$	$5.84E-03$	$6.97E+07$	$1.47E+05$	$2.89E-01$	$2.00E+00$	$1.24E+10$
1029	$1.03E+10$	$4.18E-11$	$4.29E-01$	$5.11E+09$	$1.08E+07$	$1.46E-01$	$2.00E+00$	$1.31E+10$
1046	$1.83E+10$	$3.67E-11$	$6.73E-01$	$1.61E+10$	$2.72E+07$	$2.16E-01$	$2.00E+00$	$9.86E+09$
1018	$9.65E+08$	$6.21E-10$	$5.99E-01$	$8.45E+09$	$1.79E+07$	$7.95E-01$	$0.00E+00$	$1.46E+09$
1042	$7.04E+09$	$3.29E-11$	$2.32E-01$	$1.82E+09$	$3.84E+06$	$1.70E-02$	$2.00E+00$	$1.29E+10$
1113	$3.93E+09$	$1.86E-10$	$7.32E-01$	$9.51E+09$	$2.01E+07$	$2.00E-02$	$2.00E+00$	$7.67E+09$
1053	$2.55E+09$	$1.23E-10$	$3.14E-01$	$2.11E+09$	$1.94E+06$	$8.10E-02$	$2.00E+00$	$2.02E+09$
1015	$3.39E+09$	$5.13E-11$	$1.74E-01$	$1.65E+09$	$3.49E+06$	$3.00E-03$	$3.00E+00$	$8.99E+09$
1075	$7.82E+09$	$2.06E-12$	$1.61E-02$	$4.22E+08$	$7.09E+05$	$5.85E-01$	$2.00E+00$	$7.96E+09$
1031	$1.71E+10$	$5.74E-11$	$9.81E-01$	$1.84E+10$	$3.88E+07$	$1.94E-01$	$1.00E+00$	$5.16E+09$
1036	$4.76E+08$	$1.23E-09$	$5.84E-01$	$6.16E+09$	$5.66E+06$	$6.80E-02$	$0.00E+00$	$1.21E+09$
1104	$4.86E+08$	$3.02E-10$	$1.47E-01$	$1.12E+09$	$1.03E+06$	$1.55E-01$	$0.00E+00$	$4.13E+09$
1091	$1.04E+09$	$6.43E-09$	$6.72E+00$	$1.96E+10$	$1.29E+08$	$2.53E-01$	$3.00E+00$	$6.16E+09$
1087	$7.43E+09$	$3.13E-12$	$2.33E-02$	$5.63E+07$	$1.19E+05$	$3.87E-01$	$3.00E+00$	$1.00E+10$
1045	$5.55E+09$	$7.47E-11$	$4.15E-01$	$3.14E+09$	$2.89E+06$	$1.23E-01$	$1.00E+00$	$1.11E+10$
1109	$6.07E+08$	$1.22E-10$	$7.39E-02$	$1.13E+08$	$1.04E+05$	$1.53E-01$	$1.00E+00$	$2.70E+09$
1002	$6.82E+07$	$1.20E-08$	$8.19E-01$	$8.10E+09$	$7.44E+06$	$5.47E-01$	$0.00E+00$	$1.06E+08$
1061	$7.13E+09$	$1.07E-10$	$7.61E-01$	$1.10E+10$	$2.32E+07$	$5.20E-01$	$0.00E+00$	$4.41E+09$
1022	$2.08E+07$	$2.99E-09$	$6.21E-02$	$6.03E+08$	$5.55E+05$	$2.85E-01$	$0.00E+00$	$4.59E+08$
1000	$7.95E+08$	$1.32E-10$	$1.05E-01$	$6.59E+09$	$7.02E+06$	$9.52E-01$	$5.00E+00$	$1.21E+10$
1020	$1.21E+10$	$2.72E-11$	$3.29E-01$	$2.13E+09$	$4.50E+06$	$9.00E-02$	$3.00E+00$	$1.22E+10$
1081	$1.68E+10$	$3.17E-11$	$5.32E-01$	$5.28E+09$	$4.85E+06$	$1.67E-01$	$3.00E+00$	$1.23E+10$
1074	$2.44E+09$	$3.16E-10$	$7.70E-01$	$8.63E+09$	$1.82E+07$	$7.09E-01$	$0.00E+00$	$2.24E+09$
1027	$2.13E+10$	$1.45E-11$	$3.08E-01$	$1.12E+10$	$1.75E+07$	$4.44E-01$	$0.00E+00$	$9.30E+09$
1062	$6.53E+10$	$1.91E-12$	$1.24E-01$	$4.09E+10$	$2.69E+08$	$7.74E-01$	$0.00E+00$	$8.70E+09$
1077	$1.40E+10$	$3.75E-11$	$5.24E-01$	$5.77E+09$	$1.22E+07$	$1.51E-01$	$1.00E+00$	$1.26E+10$
1028	$2.55E+09$	$1.43E-10$	$3.63E-01$	$2.32E+09$	$2.13E+06$	$5.10E-02$	$2.00E+00$	$6.27E+09$
1092	$1.43E+09$	$1.44E-10$	$2.06E-01$	$2.15E+09$	$1.98E+06$	$1.93E-01$	$1.00E+00$	$4.54E+09$
1012	$3.98E+10$	$1.82E-11$	$7.22E-01$	$1.31E+10$	$2.76E+07$	$2.70E-01$	$1.00E+00$	$1.10E+10$
1040	$8.72E+08$	$9.80E-10$	$8.55E-01$	$1.14E+10$	$2.42E+07$	$5.02E-01$	$0.00E+00$	$1.21E+09$

[a] Name from the Monnier Ragaigne, D.et al.(2003) catalog

[b] Stellar mass in $M_\odot$

[c] specific star formation ratte(yr^{-1})

[d] Star formation rate averaged over last 0.1 Gyr

[e] luminosity of dust$L_\odot$

[f] Dust mass in $M_\odot$

[g] star formation time scale

[h] no of bursts after tform

[i] age of the oldest population in Gyr